energies

MDPI

Article

Optimal Dispatch of Heterogeneous Air Conditioning Clusters for Photovoltaics Accommodation

Shilei Wu [1], Xuerui Liu [1], Ye Zhang [2], Qiang Fu [3], Chengyu Jin [1], Xun Dou [1] and Hanyu Yang [1,*]

[1] College of Electrical Engineering and Control Science, Nanjing Tech University, Nanjing 211816, China; wsl.12@njtech.edu.cn (S.W.); liuxuerui0112@163.com (X.L.); jinchengyu@njtech.edu.cn (C.J.); dxnjut@njtech.edu.cn (X.D.)
[2] Inner Mongolia Power Electric Operation Control Company, Hohhot 010000, China; 18347970528@163.com
[3] State Grid Ningbo Yinzhou Power Supply Company, Ningbo 315000, China; yzgdfq@163.com
* Correspondence: hyang73@outlook.com

Abstract

In modern power systems with high penetration of renewable energy, the efficient interaction between demand-side flexible resources and the power grid has become a key approach to mitigating renewable generation fluctuations. As a typical flexible load, air conditioning loads exhibit significant potential for renewable energy utilization due to their large scale, low cost, and fast response capability. However, existing strategies for photovoltaic (PV) accommodation fail to fully consider the coordinated scheduling between heterogeneous air conditioning clusters and energy storage systems, and lack explicit modeling of the dynamic response of air conditioning loads. As a result, they are unable to effectively address the requirements induced by renewable energy fluctuations. To address these issues, this paper proposes a coordinated scheduling strategy for heterogeneous air conditioning clusters considering dynamic response characteristics, aimed at PV fluctuation smoothing. A hierarchical framework of "fixed-frequency priority, variable-frequency compensation, and energy storage backup" is developed. By incorporating response dynamics into the scheduling process, power–energy complementarity between air conditioning clusters and energy storage systems is achieved. Experimental results demonstrate that the proposed strategy improves the PV fluctuation smoothing rate from 77.16% to 100%, significantly enhancing the local PV accommodation capability within the park.

Keywords: demand response; air conditioning; coordinated dispatch; photovoltaics accommodation

Academic Editors: Pavlos S. Georgilakis and Tapas Mallick

Received: 25 March 2026
Revised: 28 April 2026
Accepted: 11 May 2026
Published: 3 July 2026

1. Introduction

Under the guidance of the "carbon peaking and carbon neutrality" goals, constructing a new-type power system dominated by renewable energy has become a key direction for the transformation of China's energy structure. As a typical representative of distributed renewable energy, PV generation is regarded as one of the critical pathways to achieving the dual-carbon targets [1]. However, with the large-scale integration of distributed PV, its output exhibits significant variability and uncertainty, posing severe challenges to the stability of source–load coordinated regulation. Existing studies have addressed the practical need for PV accommodation and conducted extensive investigations into the regulation of PV output fluctuations, mainly focusing on energy storage technologies and the participation of large-scale air conditioning (AC) clusters in local PV accommodation.

These studies provide important theoretical support and technical means for enhancing local PV utilization and maintaining grid operational stability.

To mitigate the impact of distributed PV fluctuations on grid operation, the deployment of energy storage systems has become a widely adopted solution [2]. Among these, lithium-ion batteries, characterized by high energy density, small footprint, and short construction cycles, are commonly used in distributed PV systems [3]. However, their large-scale deployment at the park level remains constrained by high costs, limited lifespan due to deep charge–discharge cycles, and potential safety risks such as thermal runaway [4,5]. Therefore, it is necessary to explore low-cost and highly reliable flexible load resources to further improve local PV accommodation and system operational stability.

Large-scale AC clusters have gradually become a research focus for PV fluctuation smoothing due to their fast response and considerable regulation potential [6]. AC clusters can not only provide real-time responses to smooth PV power fluctuations but also enable real-time local consumption of PV generation through source–load matching. In this way, they can function as "virtual energy storage," reducing reliance on physical storage systems while improving the adaptability and economic performance of park-level energy systems. References [7,8] established virtual energy storage models for inverter air conditioners and proposed coordinated load reduction strategies based on virtual state-of-charge (SOC) ranking, achieving an effective balance among power reduction, user thermal comfort, and the mitigation of post-response load rebound. Reference [9] modeled the aggregate flexibility of thermostatically controlled loads as a stochastic battery with dissipation and proposed a priority-stack-based direct load control framework to effectively track grid regulation signals. However, existing virtual energy storage models and dispatch frameworks are typically tailored to a single type of AC load. They tend to neglect the heterogeneity inherent in practical AC populations, thereby failing to fully capture the distinct dynamic response characteristics and the coordinated scheduling potential of clusters that contain both fixed-frequency and variable-frequency units.

In recent years, research on AC clusters participating in PV fluctuation smoothing and local accommodation has been extensively conducted. Reference [10] established an aggregated AC control model considering control characteristics, comfort, and economic performance to smooth distributed generation output. Reference [11] proposed a time-of-use pricing-based control strategy for AC clusters to enhance PV utilization and reduce operational costs. Reference [12] developed a multi-timescale model predictive control framework for air-conditioning systems integrated with PV generation, enabling effective exploitation of their regulation potential to mitigate distributed generation fluctuations. Despite these advances, most existing studies focus on control strategies for a single type of AC. In practice, however, AC clusters typically consist of both fixed-frequency and variable-frequency units, which exhibit significantly different response characteristics. Applying a unified control strategy may lead to underutilization of flexibility and increased operational costs. Therefore, it is essential to develop differentiated scheduling strategies that account for the heterogeneous response behaviors of different AC types to achieve more accurate and efficient regulation.

In summary, existing studies on AC cluster scheduling for PV accommodation have made significant progress in terms of comfort preservation, economic optimization, and scheduling strategies. However, most approaches focus on homogeneous AC populations and fail to fully capture the differences in dynamic response characteristics between fixed-frequency and variable-frequency units. Moreover, systematic modeling and classification-based control of heterogeneous AC clusters are still lacking. In addition, the complementary characteristics between AC clusters and energy storage systems in terms of response capability have not been fully exploited, and coordinated scheduling mechanisms remain

insufficient. These limitations hinder effective PV accommodation and fluctuation smoothing under high variability and uncertainty. Therefore, it is necessary to explicitly model the response characteristics of fixed-frequency ACs (e.g., discrete on/off operation with minimum runtime constraints) and variable-frequency ACs (e.g., activation delay and nonlinear regulation), and to develop corresponding dynamic control models. By further integrating the power–energy regulation capability of energy storage systems to compensate for response delays and deviations, a coordinated scheduling framework of "battery–heterogeneous AC clusters" can be established, enabling precise absorption of PV fluctuations and sustained system stability.

To address the challenges, this research proposes a coordinated scheduling strategy for heterogeneous AC clusters, considering their specific dynamic response characteristics, to facilitate PV fluctuation smoothing. The novelty and main contributions of this work are summarized as follows:

1. This paper derives an exact analytical solution for the second-order ETP model, which eliminates the truncation errors and numerical instability inherent in traditional approximate recursive formulations to provide a more accurate basis for real-time AC power prediction.

2. This paper establishes a hierarchical dispatch framework of "fixed-frequency priority, variable-frequency compensation, and energy storage backup," which systematically exploits the complementary response speeds and granularities of fixed- and variable-frequency AC units to enhance overall regulation precision.

3. This paper integrates BESSs with AC clusters to compensate for response delays and deviations, achieving power–energy complementary scheduling that significantly reduces the operational intensity and energy throughput of the battery system while ensuring a 100% PV smoothing rate.

2. Energy Modeling of Energy Storage and Large-Scale Heterogeneous AC Clusters in PV Parks

The energy system framework of the PV park is illustrated in Figure 1. The PV modules and battery energy storage systems (BESSs) within the park are connected to the AC grid via inverters. The AC load fleet, comprising many variable-frequency and fixed-frequency ACs, serves as the primary energy-consuming equipment, drawing power from the AC grid.

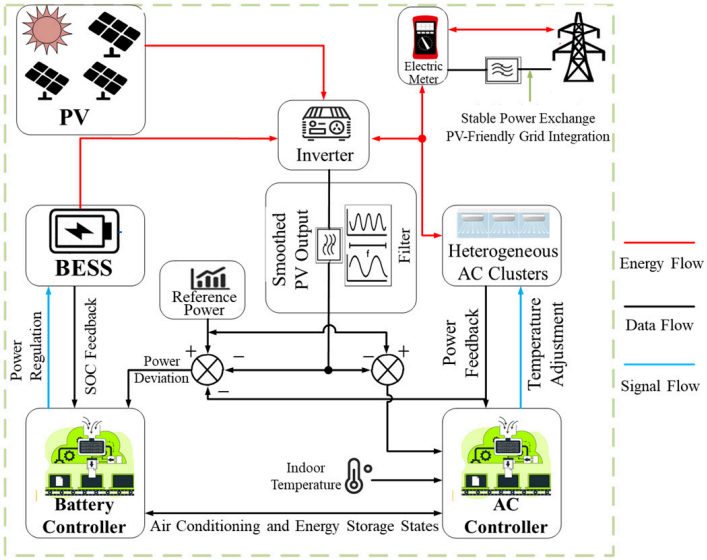

Figure 1. Energy system diagram of PV park.

To achieve grid-friendly integration of the PV park, it is essential to maintain the power stability of the tie-line between the park and the main grid. The regulation target of the tie-line power is defined as the deviation between the forecasted and actual PV power output. A load aggregator centrally coordinates the operational states of the AC load fleet and works in tandem with the BESS for energy compensation. Through their collaborative response, PV output fluctuations are effectively smoothed and locally accommodated, thereby enhancing the overall grid-friendliness of the system and fully exploiting the collaborative regulation capacity of large-scale flexible loads.

To smooth PV output fluctuations and enhance power controllability within the PV park, the system first calculates the difference between the filtered forecasted PV output and the actual PV generation. The resulting power deviation is then fed into the AC controller as the target power to regulate the AC fleet. Within the controller, the temperature setpoints of the AC units are dynamically adjusted based on current indoor temperature conditions and the real-time operating power of the ACs, thereby achieving responsive regulation of the AC load fleet. If the regulation capacity of the AC fleet is insufficient to fully accommodate the PV power deviation, the remaining deviation is compensated by the BESS through its charging and discharging processes. Through the coordinated scheduling of the AC fleet and the BESS, the system effectively enhances the stability of the tie-line power with the main grid while guaranteeing indoor thermal comfort. The system components within the park and their characteristics are summarized in Table 1.

Table 1. Characteristics of the System Components.

System Component	Characteristics
PV	Stochastic and intermittent power generation; primary renewable energy source sensitive to weather conditions.
BESS	High-density energy storage with rapid bi-directional power response and smoothing capabilities.
Battery Controller	Manages SOC and power output to ensure safe, stable, and efficient battery operation.
AC Controller	Executes local temperature set-point adjustments and facilitates real-time data communication.
Heterogeneous AC Clusters	Aggregates demand-side flexibility; characterized by diverse Equivalent Thermal Parameter models.

2.1. Modeling of Room Thermal Dynamics and Multi-Type Heterogeneous Air Conditioners

The thermal inertia of indoor spaces is strongly coupled with the regulation capability of air conditioning systems, while dynamic variations in outdoor meteorological conditions lead to time-varying responses in the operating power of air conditioning units. To develop a demand response-based dynamic scheduling strategy for air conditioning power, it is necessary to establish a high-accuracy real-time prediction model of the indoor thermal environment. When the indoor temperature deviates from the preset comfort range, the air conditioning system should appropriately adjust the temperature setpoint to maintain occupant thermal comfort.

(1) Second-Order Equivalent Thermal Parameter (ETP) Model

Since the first-order ETP model neglects the solid temperature, it introduces certain inaccuracies in characterizing indoor air thermal dynamics. Considering that indoor objects, furnishings, and the building structure possess inherent heat storage and release

capabilities, the second-order model extends the first-order formulation by incorporating the thermal resistance and thermal capacitance associated with indoor solid components, as well as explicitly modeling the indoor solid temperature. Consequently, it can more accurately capture the thermodynamic characteristics of individual air conditioning units [13]. The second-order equivalent thermal parameter model is illustrated in Figure 2.

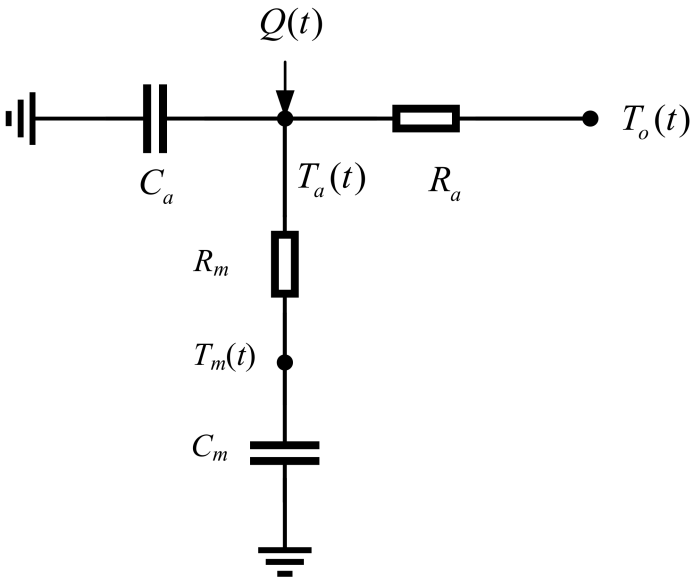

Figure 2. Equivalent thermal parameter model of single second-order air conditioning.

The second-order ETP model of an individual air conditioning unit can be described by the following set of differential equations:

$$\begin{cases} \frac{dT_a(t)}{dt} = -\frac{1}{C_a}\left(\frac{1}{R_a} + \frac{1}{R_m}\right)T_a(t) + \frac{1}{C_a R_m}T_m(t) + \frac{1}{C_a}\left(\frac{T_o(t)}{R_a} + Q(t)\right) \\ \frac{dT_m(t)}{dt} = \frac{1}{C_m R_m}T_a(t) - \frac{1}{C_m R_m}T_m(t) \end{cases} \quad (1)$$

where R_a, C_a and R_m, C_m denote the equivalent heat capacities and thermal resistances of the indoor air and solid mass, respectively; $T_a(t)$ is the indoor air temperature; $T_m(t)$ is the inner solid temperature; $T_o(t)$ is the outdoor ambient temperature; and $Q(t)$ represents the heating power of the air conditioner. Specifically, R_m denotes the equivalent thermal conduction resistance of the building envelope (e.g., walls and roofs), reflecting the obstruction of building materials to heat transfer. C_m represents the heat storage capacity of the building materials. A higher value of C_m indicates stronger thermal inertia of the building envelope, which can significantly decelerate the transmission rate of outdoor temperature disturbances into the room. During the AC response process, this characteristic manifests as follows: when the AC switches its operating status or regulates its power, a higher C_m prolongs the dynamic response latency of the indoor temperature, reduces the state-switching frequency of the AC triggered by short-term temperature fluctuations, and extends the stable time window within the temperature thresholds. Consequently, this provides a more flexible operational and regulatory space for power grid demand response.

To numerically solve the second-order ETP model, conventional studies predominantly adopt approximate recursive formulations. Such formulations are essentially linearized approximations of the model under small time-step conditions. Consequently, inherent errors are introduced and continuously accumulate in each recursive step. Moreover, the error amplifies with the increase in the time step Δt_k. When Δt_k exceeds a certain threshold, the approximate recursive formulation may exhibit numerical oscillation or even diverge [14].

To address the aforementioned issues and enhance both the accuracy and numerical stability of parameter identification for the second-order ETP model, this paper introduces its exact analytical solution.

If the inputs $T_o(t)$ and $Q(t)$ remain constant over a given time interval, Equation (1) can be regarded as a system of second-order non-homogeneous linear differential equations with constant coefficients. Its general solution can be derived by solving the characteristic equation. The calculation procedure is as follows:

By rearranging the derivative terms in Equation (1), we yield:

$$T_a(t) = T_m(t) + C_m R_m \frac{dT_m(t)}{dt} \tag{2}$$

Substituting Equation (2) into Equation (1) to eliminate $T_a(t)$, and rearranging the terms, we obtain:

$$\begin{aligned} &\frac{d^2T_m(t)}{dt^2} + \left(\frac{1}{C_aR_a} + \frac{1}{C_aR_m} + \frac{1}{C_mR_m}\right)\frac{dT_m(t)}{dt} + \frac{1}{C_aC_mR_aR_m}T_m(t) \\ &= \frac{1}{C_aC_mR_m}\left(\frac{T_o(t)}{R_a} + Q(t)\right) \end{aligned} \tag{3}$$

Setting the characteristic equation as:

$$r^2 + br + c = 0 \tag{4}$$

where $b = (1/C_aR_a + 1/C_aR_m + 1/C_mR_m)$; $c = 1/C_aC_mR_aR_m$.

Consequently, the analytical solution for $T_m(t)$ is given by:

$$T_m(t) = C_1e^{r_1t} + C_2e^{r_2t} + T_o(t) + Q(t)R_a \tag{5}$$

where $r_1 = \frac{-b+\sqrt{b^2-4c}}{2}$; $r_2 = \frac{-b-\sqrt{b^2-4c}}{2}$.

Similarly, we can obtain:

$$T_a(t) = T_m(t) + C_mR_m\frac{dT_m(t)}{dt} = (C_mR_mC_1r_1 + C_1)e^{r_1t} + (C_mR_mC_2r_2 + C_2)e^{r_2t} + T_o(t) + Q(t)R_a \tag{6}$$

The initial conditions at time t_k are given by:

$$T_a(t_k) = C_mR_m(C_1r_1 + C_2r_2) + C_1 + C_2 + T_o(t_k) + Q(t_k)R_a \tag{7}$$

$$T_m(t_k) = C_1 + C_2 + T_o(t_k) + Q(t_k)R_a \tag{8}$$

Then, C_1 and C_2 can be expressed in terms of $T_a(t_k)$ and $T_m(t_k)$ as:

$$C_1 = \frac{\frac{T_a(t_k)-T_m(t_k)}{C_mR_m} + [(T_o(t_k) + Q(t_k)R_a) - T_m(t_k)]r_2}{\sqrt{b^2-4c}} \tag{9}$$

$$C_2 = \frac{\frac{T_a(t_k)-T_m(t_k)}{C_mR_m} + [(T_o(t_k) + Q(t_k)R_a) - T_m(t_k)]r_1}{-\sqrt{b^2-4c}} \tag{10}$$

Therefore, Equations (7) and (8) can be rewritten as:

$$\begin{aligned} T_a(t_{k+1}) = {} & \frac{\left(r_1+\frac{1}{C_mR_m}\right)e^{r_1\Delta t_k} - \left(r_2+\frac{1}{C_mR_m}\right)e^{r_2\Delta t_k}}{\sqrt{b^2-4c}}T_a(t_k) + \frac{\left(\frac{1}{C_aR_m}\right)\left(e^{r_1\Delta t_k} - e^{r_2\Delta t_k}\right)}{\sqrt{b^2-4c}}T_m(t_k) \\ & + \left[1 + \frac{\left(\frac{1}{C_aR_a}+r_2\right)e^{r_1\Delta t_k} - \left(\frac{1}{C_aR_a}+r_1\right)e^{r_2\Delta t_k}}{\sqrt{b^2-4c}}\right](T_o(t_k) + Q(t_k)R_a) \end{aligned} \tag{11}$$

$$T_m(t_{k+1}) = \frac{1}{C_m R_m \sqrt{b^2-4c}}(e^{r_1\Delta t_k} - e^{r_2\Delta t_k})T_a(t_k) + \left[\frac{1}{C_m R_m}(e^{r_2\Delta t_k} - e^{r_3\Delta t_k}) + r_1 e^{r_2\Delta t_k}\right]\frac{T_m(t_k)}{\sqrt{b^2-4c}} + (1 + \frac{r_2 e^{r_1\Delta t_k} - r_1 e^{r_2\Delta t_k}}{\sqrt{b^2-4c}})(T_o(t_k) + Q(t_k)R_a) - \frac{T_m(t_k) r_2 e^{r_1\Delta t_k}}{\sqrt{b^2-4c}} \quad (12)$$

In summary, the discrete forms of the analytical solution for the second-order ETP model are presented in Equations (11) and (12), which parametrically characterize the energy transfer and decay processes within the Resistor–Capacitor (RC) network via exponential terms. Compared to the coefficient simplification inherent in approximate recursive formulations, these exponential terms directly reflect the coupling effects of thermal resistance and capacitance in the RC circuit. This enables a precise representation of the dynamic temperature transfer rates between the air and solid dual nodes, effectively guaranteeing the asymptotic convergence of the analytical solution. Furthermore, this formulation is highly adaptable, simultaneously satisfying the step-response modeling requirements of fixed-frequency ACs and the continuous parameter updating demands of variable-frequency Acs.

(2) Operating model of AC loads

Assuming the AC temperature setpoint of room h is $T_{set}^{(h)}$, the actual indoor temperature $T_a^{(h)}$ operates within the interval of $[T_{set}^{(h)} - T_\delta^{(h)}, T_{set}^{(h)} + T_\delta^{(h)}]$. Here, $T_\delta^{(h)}$ denotes the temperature deadband, representing the maximum allowable deviation between the actual temperature $T_a^{(h)}$ and the setpoint $T_{set}^{(h)}$. Taking an AC operating in the cooling mode as an example, the temperature variation trajectory is illustrated in Figure 3a.

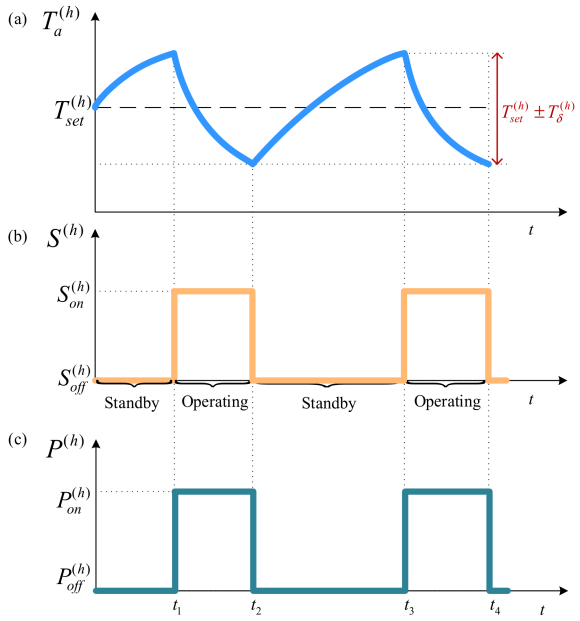

Figure 3. The operating characteristics of single air conditioner: (**a**) set temperature and actual room temperature; (**b**) Operational status; (**c**) Operating power.

When employing the hysteresis scheduling strategy, the AC switches between the cooling state $S_{on}^{(h)}$ and the standby state $S_{off}^{(h)}$ during operation, as illustrated in Figure 3b. When the indoor temperature $T_a^{(h)}$ is lower than or equal to the minimum temperature limit $T_{set}^{(h)} - T_\delta^{(h)}$, the AC enters the standby state $S_{off}^{(h)}$. When $T_a^{(h)}$ is higher than or equal to the maximum temperature limit $T_{set}^{(h)} + T_\delta^{(h)}$, the AC enters the cooling state $S_{on}^{(h)}$. However, when the temperature falls between the upper and lower limits—i.e., within the tempera-

ture deadband—the state of the AC compressor does not transition. Instead, it maintains its operating state from the previous time step, yielding $S = S(t_{k-1})^{(h)}$.

$$S(t_k)^{(h)} = \begin{cases} 1, & T_a^{(h)} \geq T_{set}^{(h)} + T_\delta^{(h)} \\ 0, & T_a^{(h)} \leq T_{set}^{(h)} - T_\delta^{(h)} \\ S(t_{k-1})^{(h)}, & T_{set}^{(h)} - T_\delta^{(h)} < T_a^{(h)} < T_{set}^{(h)} + T_\delta^{(h)} \end{cases} \tag{13}$$

The compressor, serving as the core of the cooling/heating system, is the primary power-consuming component of an air conditioner. Based on the operating state of the AC, its electrical power consumption can be categorized into cooling power $P_{on}^{(h)}$ and standby power $P_{off}^{(h)}$, as illustrated in Figure 3c, which is expressed as:

$$P^{(h)} = \begin{cases} P_{on}^{(h)}, S_{on}^{(h)} \\ P_{off}^{(h)}, S_{off}^{(h)} \end{cases} \tag{14}$$

2.2. Modeling of Battery Energy Storage Systems

Energy storage systems primarily include battery, flow battery, pumped hydro, compressed air, and flywheel energy storage. Among these, lead-acid batteries are currently one of the most widely applied energy storage technologies due to their relatively low cost, as well as their convenient installation and operational management.

BESSs typically use the State of Charge (SOC) as the primary metric to quantify their stored energy. SOC is defined as the ratio of the remaining capacity in the energy storage system to its rated capacity, accurately reflecting the charging and discharging status of the battery. The remaining capacity of the battery at time t is determined by the capacity at the previous time step and the amount of charge or discharge during the time interval $[t-1, t]$. The mathematical expression is given by:

$$SOC(t) = SOC(t-1) + E_{BESS}(t-1)/R_{BESS} \tag{15}$$

where $SOC(t)$ is the initial state of charge at time t; $E_{BESS}(t-1)$ represents the charging or discharging capacity of the battery during time step $t-1$, which is positive during charging and negative during discharging; and R_{BESS} is the rated capacity of the battery energy storage system.

Overcharging or deep discharging during operation can adversely affect the lifespan of a battery. To prolong the battery's service life and ensure the stable operation of the system, the SOC of the BESS is typically constrained. It is restricted to operate within predefined upper and lower limits to prevent extreme operating conditions from degrading battery performance. This constraint can be expressed as:

$$SOC_{\min} \leq SOC(t) \leq SOC_{\max} \tag{16}$$

where $SOC_{\min}$ and $SOC_{\max}$ are the predefined minimum and maximum limits of the SOC, respectively. The upper and lower limits of the SOC are defined based on typical industry standards for lithium-ion batteries to prevent overcharging and deep discharging, thereby balancing battery longevity with the operational reliability of the system.

The charging and discharging power of the battery is governed not only by its inherent electrochemical characteristics but also by the capacity of its associated inverter. Consequently, in practical operation, its charging and discharging capabilities must simul-

taneously satisfy the dual constraints imposed by the battery's physical performance and the capacity of the power conversion equipment. This can be expressed as:

$$P_{charge,\max} = \min(R_{inv}, \alpha_{inv} P_{charge}) \tag{17}$$

$$P_{discharge,\max} = \min(R_{inv}, P_{discharge}) \tag{18}$$

where $P_{charge,\max}$ and $P_{discharge,\max}$ are the maximum charging and discharging powers of the battery, respectively; R_{inv} is the capacity of the inverter; and P_{charge}, $P_{discharge}$ represent the inherent charging and discharging powers of the battery itself, respectively.

During any given time interval, the maximum charging and discharging energy of the energy storage system is determined by both its maximum charging and discharging power limits and its current SOC. This can be expressed as:

$$E_{BESScha,\max}(t) = \min(P_{charge,\max}\Delta t, (SOC_{\max} - SOC(t))R_{BESS}) \tag{19}$$

$$E_{BESSdis,\max}(t) = \min(P_{discharge,\max}\Delta t, (SOC(t) - SOC_{\min})R_{BESS}) \tag{20}$$

where $E_{BESScha,\max}(t)$ and $E_{BESSdis,\max}(t)$ are the maximum charging and discharging energy of the battery energy storage system, respectively.

3. Operational Scheduling Strategy for Heterogeneous ACs in PV Parks

3.1. Scheduling Strategy for Grid-Friendly PV Integration

In PV parks with large installed capacities, the photovoltaic power output is highly susceptible to localized irradiance variations caused by surrounding obstacles, leading to significant fluctuations. Such high-frequency fluctuations force the AC system to frequently adjust its temperature setpoints. Furthermore, relying entirely on energy storage devices to smooth these fluctuations presents limitations in terms of both economic efficiency and system stability.

Given that the power grid possesses a certain tolerance for minor fluctuations, the actual PV output can be processed through a moving average filter to eliminate high-frequency components. This yields a smoothed PV power as $P^s_{PV}(t)$, expressed as follows, where n represents the number of sampling points used for the moving average:

$$P^s_{PV}(t) = \frac{1}{n}\sum_{i=0}^{n} P_{PV}(t-i) \tag{21}$$

By utilizing the filtered and smoothed PV output as the scheduling input, a composite energy storage system—comprising the coordinated BESS and multi-type heterogeneous AC fleets—is constructed. This system is designed to compensate for the deviation between the smoothed PV output and the forecasted PV output, thereby achieving the grid-friendly integration of PV generation. The scheduling objective is to minimize the deviation $\Delta P_l(t)$ between the actual power and the forecasted power on the tie-line connecting the park to the main grid, which is expressed as:

$$\Delta P_l(t) = P_{line}(t) - P^m_{line}(t) = 0 \tag{22}$$

$$P_{line}(t) = P^s_{PV}(t) + P_{bat}(t) - P_{ACG}(t) - P_{IACG}(t) - P_L(t) \tag{23}$$

$$P^m_{line}(t) = P^m_{PV}(t) - P^m_{ACG}(t) - P^m_{IACG}(t) - P^m_L(t) \tag{24}$$

where $P_{line}(t)$ and $P^m_{line}(t)$ represent the actual power and forecasted power of the tie-line, respectively, with positive values indicating power injected into the grid and negative values indicating power purchased from the grid; $P_{bat}(t)$ represents the real-time power of

the battery (positive for discharging, negative for charging); $P_{ACG}(t)$, $P_{IACG}(t)$, and $P_L(t)$ are the real-time total powers of the fixed-frequency AC fleet, variable-frequency AC fleet, and other energy-consuming loads, respectively. Furthermore, $P_{PV}^{m}(t)$ is the forecasted PV output; and $P_{ACG}^{m}(t)$, $P_{IACG}^{m}(t)$, and $P_{L}^{m}(t)$ are the forecasted powers of the fixed-frequency AC fleet, variable-frequency AC fleet, and other appliances, respectively. Assuming the other loads are predetermined, the scheduling objective, namely the target power, can be simplified as:

$$P_{\text{target}} = P_{PV}^{s}(t) - P_{PV}^{m}(t) \tag{25}$$

The energy optimization process of the PV park is illustrated in Figure 4. First, based on the room structural parameters, indoor and outdoor temperatures, and current temperature setpoints, and subsequently utilizing the collected real-time data, filtered PV output, and target scheduling power, the required temperature adjustment amounts for both the fixed-frequency and variable-frequency AC fleets are determined.

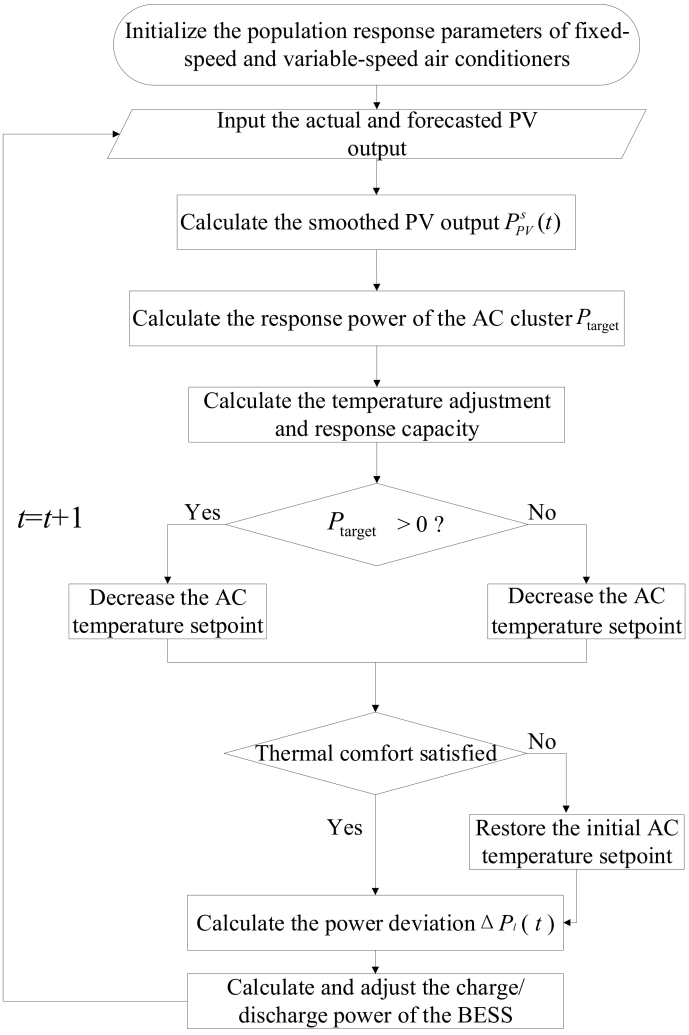

Figure 4. PV integration park energy optimization operation flow chart.

Based on the target power, the required magnitude of the setpoint temperature adjustment and the response scale of the AC fleets are calculated. The fixed-frequency and variable-frequency AC fleets are then regulated according to their respective differentiated scheduling strategies to smooth the fluctuations caused by the PV output. During the response process, the real-time power of the system is prone to deviations due to the discrete nature of AC load regulation and the uncertainty of response latency. Conse-

quently, the energy storage system dynamically intervenes based on a "Battery-AC Fleet Power and Energy Complementary Scheduling Strategy." By precisely compensating for the AC response deviations, a composite coordinated regulation between the AC fleets and the energy storage system is achieved, thereby enhancing the tracking accuracy and accommodation capacity for PV power fluctuations.

3.2. Temperature Scheduling Strategy for Large-Scale Fixed-Frequency AC Fleets Based on Optimal Selection of Response States

To address the characteristics of fixed-frequency ACs, such as discrete ON/OFF operations, response latency, and minimum ON/OFF time constraints, this paper proposes a fleet setpoint temperature scheduling strategy based on response state identification and priority ranking, built upon the established models. By identifying the current operational state, temperature deviation, and ON/OFF timing status of individual AC units, this strategy constructs hierarchical response sets and performs priority ranking. It selectively adjusts the temperature setpoints of specific ACs to achieve precise regulation of the fleet's aggregate power, thereby laying the foundation for the AC fleet to participate in fast power regulation tasks, such as PV accommodation.

(1) Optimal Selection Mechanism for Response States

To enhance the accuracy and effectiveness of the regulation strategy for the AC load fleet, this paper introduces an optimal selection mechanism for response states, which selects the most suitable units from the AC fleet for adjustment based on current regulation requirements.

First, based on the current operational conditions and the ON/OFF lockout status of the AC units, the AC fleet is divided into hierarchical state sets, as shown in Figure 5. Specifically, the AC states can be classified into the following four categories:

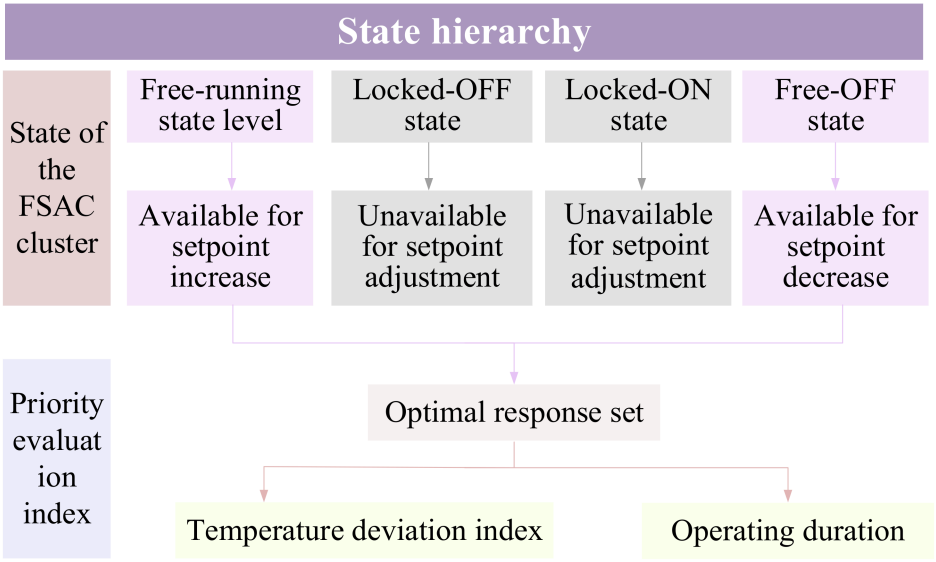

Figure 5. Response state optimization mechanism of fixed-frequency air-conditioning cluster.

Free-layer running state: ACs that are currently operating and are not bound by the minimum ON/OFF time lockout constraints. These units possess significant downward power regulation potential; by increasing their temperature setpoints, they can be immediately shut down to achieve load reduction.

Free-layer standby state: ACs that are currently in standby and are not bound by the minimum OFF time constraints. These units possess upward power regulation capacity; by decreasing their temperature setpoints, their compressors can be immediately started to achieve a load increase.

Locked-layer running state: ACs that are currently operating but have not yet satisfied the minimum continuous ON time and thus cannot be interrupted. Even if the target temperature is reached, these units must continue to operate and temporarily lack response capability.

Locked-layer standby state: ACs that are currently shut down and have not yet satisfied the minimum OFF time. These units are in a lockout period, cannot be restarted via temperature setpoint adjustments, and are consequently excluded from the current response scope.

The aforementioned classification ensures that all AC units within the response candidate set satisfy the ON/OFF constraints, thereby avoiding the adverse impacts of frequent starting and stopping on equipment lifespan and operational stability. For a large-scale AC fleet, an optimal selection mechanism for response states must be integrated into the scheduling strategy. This mechanism ranks the response priority indices based on the operational parameters of the ACs and the degree of impact on user comfort, thereby screening target units with higher responsiveness for regulation. This mechanism primarily considers the following two indices:

Temperature Difference Index (ΔT_q): This represents the difference between the current indoor temperature and the temperature setpoint of the AC, reflecting the proximity of the unit to the thermostat's ON/OFF threshold. For ACs in the running state, a smaller ΔT_q (or even a negative value, indicating that the room temperature has already dropped below the setpoint) signifies that the unit is approaching its natural shutdown state. Prematurely shutting down such units has a minimal impact on indoor temperature and user comfort; hence, they should be assigned a higher priority for load reduction. Conversely, a running AC with a large ΔT_q (where the room temperature is well above the setpoint) indicates that the room has not yet reached the target temperature and user demand is unmet, making it unsuitable for immediate shutdown. For ACs in the standby state, a negative ΔT_q (room temperature below the setpoint) indicates that the room remains relatively cool and does not require the compressor to start in the short term. However, if ΔT_q is close to zero or positive (room temperature reaching or exceeding the setpoint), it indicates that the AC will soon need to initiate cooling. Therefore, such ACs should be prioritized when selecting units to increase the load.

$$\Delta T_i = T_a - T_{set} \tag{26}$$

Operating Duration Index (τ_q): This refers to the continuous duration for which the AC has been in its current running or standby state. For ACs in the running state, a longer τ_q indicates that the unit has been continuously providing cooling for an extended period, meaning a certain amount of cooling capacity has accumulated indoors, granting it a higher potential for load reduction. A short-term shutdown operation has a relatively minor impact on user comfort while simultaneously helping to alleviate the decline in energy efficiency and hardware fatigue caused by prolonged continuous operation. Therefore, such units should be assigned a higher priority in load reduction responses. For ACs in the standby state, a longer τ_q indicates a prolonged shutdown, meaning the room temperature may have rebounded close to the setpoint, thereby exhibiting a higher need for restarting. When the system requires rapid upward load regulation (e.g., during a sudden drop in PV output), such units can serve as priority candidates for startup to achieve rapid load compensation.

To further enhance the precision and flexibility of load regulation, this paper introduces a response priority evaluation index based on the temperature difference states and operational timing characteristics. This enables the refined screening and ranking of the free-layer ACs.

For ACs currently in the running state that have satisfied the minimum continuous ON time requirement, their response potential is primarily manifested in the ability to increase their temperature setpoints, thereby inducing premature shutdown and achieving load reduction. The load reduction priority index for this type of unit is expressed as follows:

$$\Gamma_q^{\downarrow} = w_1^{\downarrow} \cdot \left(1 - \frac{\Delta T_q}{T_\delta}\right) + w_2^{\downarrow} \cdot \frac{\tau_q^{on}}{\tau_{\max}^{on}} \tag{27}$$

where $w_1^{\downarrow}$ and $w_2^{\downarrow}$ are weighting coefficients, which can be adjusted based on the practical emphasis on thermal comfort versus energy efficiency; τ_q^{on} is the current continuous operating duration; $\tau_{\max}^{on}$ is Maximum operating time; and $\Gamma_q^{\downarrow}$ is the load reduction priority index.

For individual AC units currently in the standby state, their primary regulatory role is to increase the system load. The load increase priority index for this type of unit is expressed as follows:

$$\Gamma_q^{\uparrow} = \begin{cases} w_1^{\uparrow} \frac{\Delta T_q}{\Delta T_{\max}} + w_2^{\uparrow} \frac{\tau_q^{off}}{\tau_{\max}^{off}}, & \Delta T_q > 0 \\ 0 \quad , & \Delta T_q \le 0 \end{cases} \tag{28}$$

where $w_1^{\uparrow}$ and $w_2^{\uparrow}$ are weighting coefficients; τ_q^{off} is the current continuous standby duration; $\tau_{\max}^{off}$ is Maximum off time; and $\Gamma_q^{\uparrow}$ is the load increase priority index.

(2) Dynamic Temperature Setpoint Adjustment Strategy

Once the screening of the responsive AC fleet is complete, the scheduling strategy induces these ACs to alter their ON/OFF states by adjusting their temperature setpoints. Specifically, for ACs that require shutdown, the scheduling command increases the temperature setpoint by $\Delta T_{set}^{\uparrow}$; for ACs that require startup, the scheduling command decreases the temperature setpoint by $\Delta T_{set}^{\downarrow}$. The magnitude of the temperature adjustment is dynamically determined based on real-time regulation requirements and the current states of the ACs.

During the continuous regulation process, the temperature setpoint of a single AC unit can be adjusted in multiple steps according to dynamically changing system requirements. If the PV output continues to decline, necessitating further AC load reduction, the temperature setpoints of the already-shutdown ACs can be slightly increased again at subsequent time steps to prolong their OFF times, and vice versa. Conversely, if the external demand reverses (e.g., an increase in load is required to accommodate surplus PV generation), the previously increased temperature setpoints can be gradually restored or lowered in a timely manner to reactivate certain AC units. Through this iterative temperature adjustment approach, the regulation of the fleet's aggregate power is achieved. Furthermore, the temperature setpoint of each AC must be constrained within the user-permitted comfort range and gradually restored to the user's original setpoint after the regulation concludes, thereby guaranteeing user comfort and the sustainability of the scheduling strategy.

Through the aforementioned mechanism, the scheduling strategy avoids simply broadcasting a uniform temperature adjustment amount to all ACs. Instead, it applies differentiated setpoint adjustments to specific units. This strategy can precisely induce targeted ACs to undergo ON/OFF state transitions, thereby driving the fleet's aggregate power to track the expected variations.

(3) Power Response Characteristics and Scheduling Process of Fixed-Frequency AC Fleets

The power response characteristics of a large-scale AC fleet under the aforementioned regulation strategy can be characterized by the changes in the ON/OFF states of individual AC units within the fleet. Assuming the AC fleet consists of N units, the power consumed

by each fixed-frequency AC during operation is its rated power $P_{AC,i}$, and its power during shutdown is approximately zero. Consequently, the aggregate power of the fleet at time t is the sum of the operational state indicators of all individual ACs, expressed as:

$$P_{ACG}(t) = \sum_{i=1}^{N} s_i(t) \cdot P_{AC,i} \tag{29}$$

where $s_i(t)$ is the ON/OFF state indicator function of AC i at time t, with $s_i = 1$ indicating the running state and $s_i = 0$ indicating the standby state. Since fixed-frequency ACs operate exclusively in two discrete states (ON/OFF), the above equation demonstrates that the aggregate fleet power is directly proportional to the number of operating AC units. By adjusting the temperature setpoints of specific ACs, the scheduling commands alter their respective s_i states, which directly maps to an increase or decrease in the aggregate fleet power. However, due to the latency and uncertainty inherent in the AC ON/OFF transitions, the actual aggregate power of the fleet will exhibit a specific transient response process.

The scheduling logic steps for the large-scale fixed-frequency AC fleet are as follows:

(1) Calculate Demand Power Deviation: Obtain upper-level dispatch commands or local PV output variations in real time to determine the required power increment $\Delta P_{ACG}(t)$ for the AC fleet at the current time step (a positive value indicates the need to increase the load to absorb power, while a negative value indicates the need to reduce the AC load).

(2) Optimal Selection of Response States: Collect current state information for each unit within the AC fleet, including operational status (running/standby), indoor and setpoint temperatures, and their respective continuous operating/standby durations. Based on the optimal selection mechanism for response states described above, classify the ACs and generate a response priority list. For scenarios requiring load reduction (when $\Delta P_{ACG}(t) < 0$), traverse the priority list of running ACs from highest to lowest, marking selected ACs for shutdown until the accumulated reducible power approaches the target. Conversely, when a load increase is required (when $\Delta P_{ACG}(t) > 0$), perform the identical screening process on standby ACs to generate a set of ACs pending startup.

(3) Allocate Regulation Commands: Issue the corresponding temperature setpoint adjustment commands according to the selected set of ACs pending regulation. The temperature adjustment magnitude ΔT_{set} for each AC can be dynamically set based on the magnitude of $\Delta P_{ACG}(t)$. If the magnitude of $\Delta P_{ACG}(t)$ is small, prioritize minor adjustments to a select few ACs with the highest priority; if $\Delta P_{ACG}(t)$ is large, expand the number of ACs participating in the regulation, and if necessary, increase the temperature adjustment magnitude for specific ACs to ensure sufficient aggregate response capacity. The commands assigned to different ACs are mutually independent and are formulated based on their individual state characteristics.

3.3. Temperature Scheduling Strategy for Large-Scale Variable-Frequency AC Fleets Based on Piecewise Hysteresis

In the regulation scenario aimed at mitigating PV power fluctuations within the park, variable-frequency AC fleets serve as continuously adjustable flexible load resources, possessing robust fine-grained regulation capabilities. Compared to the binary ON/OFF characteristics of fixed-frequency ACs, variable-frequency ACs can achieve smoother load regulation. They primarily achieve this by adjusting temperature setpoints to indirectly modulate the compressor's operating frequency, thereby altering the power consumption per unit time and enabling a dynamic response to the system-side power demand.

However, constrained by the inherent scheduling characteristics of variable-frequency ACs, their power regulation process exhibits discrete, step-like variation patterns. Particularly in cooling mode, the power output of the variable-frequency compressor does not

respond linearly to minor changes in the temperature setpoint; rather, it manifests typical temperature-driven piecewise response characteristics. As illustrated by the red line in Figure 6, when the power deviation increases to $\Delta P_{T-1}^{IAC}/2$, if the AC's temperature setpoint is reduced by 1 °C, the power deviation will subsequently change to $\Delta P_{T+1}^{IAC}/2$.

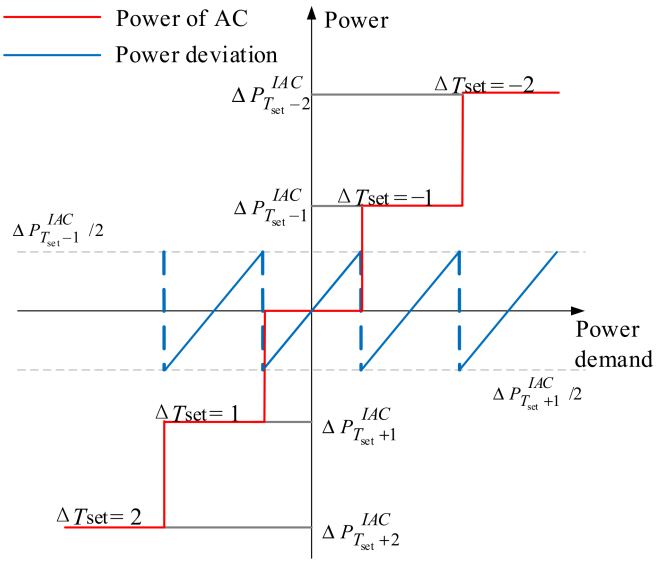

Figure 6. Response power deviation of inverter air conditioner.

Evidently, because the temperature setpoint is a discrete variable and the compressor regulation exhibits non-linear regions, the unit power adjustment of variable-frequency ACs possesses a distinct granular nature, making it difficult to achieve precise tracking of a continuous target power. Therefore, when participating in the real-time load regulation of distributed PV systems, a non-negligible response deviation exists between their actual output power and the expected regulation value. This can cause the aggregate response power to deviate from the target range, thereby degrading the compensation accuracy for PV power fluctuations.

To more accurately characterize the response latency and the non-linear power regulation patterns of variable-frequency ACs during actual operation, as well as to reflect their scalability in fleet modeling, this paper proposes a temperature difference-driven piecewise hysteresis scheduling strategy. Furthermore, it constructs a unified response regulation mechanism designed for large-scale variable-frequency AC fleets.

(1) Principle of the Scheduling Strategy

To address the discontinuity of the response power inherent in the actual operation of variable-frequency ACs, it is first necessary to quantify their corresponding response power under various magnitudes of temperature setpoint adjustments.

Given known room structural parameters and defined AC equipment characteristics, and assuming the outdoor ambient temperature remains constant during the response process, once the temperature setpoint is altered and the system re-enters steady-state operation, the variation between the new AC power and the pre-regulation steady-state power can be simplified as:

$$\Delta P_{T_{set}+\Delta T_{set}}^{IAC} = M_{IAC}\frac{\Delta T_{set}}{\eta_{IAC}R_aC_a} \tag{30}$$

where M_{IAC} is the operating mode of the AC, -1 for cooling mode, 1 for heating mode; $\Delta P_{T_{set}+\Delta T_{set}}^{IAC}$ represents the power variation in the AC after its temperature setpoint is adjusted from T_{set} to $(T_{set}+\Delta T_{set})$, with values less than zero indicating a decrease in AC

power and positive values indicating an increase; and η_{IAC} is the energy efficiency ratio of the variable-frequency AC.

As indicated by Equation (30), assuming the outdoor temperature remains constant, the power variation in the AC in cooling mode is inversely proportional to the magnitude of the temperature setpoint adjustment. However, following a change in the temperature setpoint, the AC does not instantaneously adjust to the new power level. Instead, an "activation time delay" phenomenon occurs. Furthermore, a smaller magnitude of temperature adjustment results in a lower response rate and a slower power variation process, exhibiting a distinct response lag.

Therefore, to achieve a favorable balance between response speed and regulation stability, this paper introduces a temperature difference-driven piecewise hysteresis scheduling strategy to optimize the regulation behavior of the AC fleet. Meanwhile, to account for user comfort constraints, the magnitude of the temperature setpoint adjustment is restricted within a finite range, typically set to ± 1 °C or ± 2 °C. This ensures the aggregate response capacity of the fleet is met while preventing excessive fluctuations in indoor temperature, thereby enhancing the acceptability and practical feasibility of the regulation strategy. The logic of the piecewise hysteresis temperature difference scheduling is as follows:

$$\Delta T_{set} = \begin{cases} 2\ ^\circ\text{C}, \Delta P_{IAC} < \Delta P^{\text{IAC}}_{T_{set}+2.5} \\ 1\ ^\circ\text{C}, \Delta P^{\text{IAC}}_{T_{set}+1.5} < \Delta P_{IAC} \le \Delta P^{\text{IAC}}_{T_{set}+2.5} \\ 0\ ^\circ\text{C}, \Delta P^{\text{IAC}}_{T_{set}-1.5} < \Delta P_{IAC} \le \Delta P^{\text{IAC}}_{T_{set}+1.5} \\ -1\ ^\circ\text{C}, \Delta P^{\text{IAC}}_{T_{set}-2.5} < \Delta P_{IAC} \le \Delta P^{\text{IAC}}_{T_{set}-1.5} \\ -2\ ^\circ\text{C}, \Delta P_{IAC} \ge \Delta P^{\text{IAC}}_{T_{set}-2.5} \end{cases} \tag{31}$$

The specific scheduling flow is illustrated in Figure 7. In the figure, the black solid line represents the typical mapping relationship between the variation in the AC temperature setpoint and its response power, reflecting the piecewise characteristics of the power regulation. The blue dashed line corresponds to the regulatory behavior when the temperature setpoint is decreased, while the orange dashed line represents the regulatory behavior when the temperature setpoint is increased. This figure demonstrates the non-linear variation trend of the AC power response with respect to the magnitude of the temperature adjustment under different regulation directions, thereby providing theoretical support and a basis for the subsequent design of response strategies and fleet regulation.

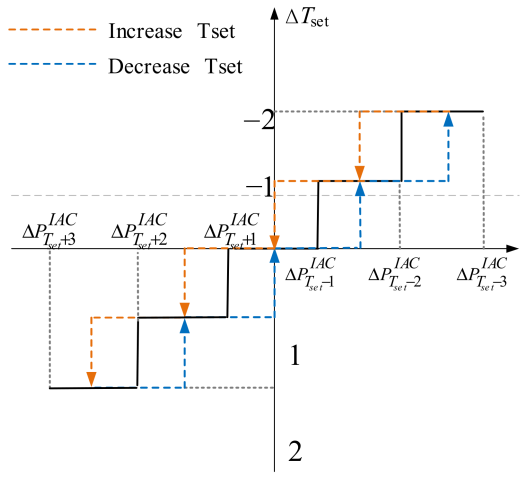

Figure 7. Variable frequency air conditioning segmented hysteresis temperature scheduling chart.

Taking the load increase scenario as an example, when the power deviation ΔP_{IAC} is greater than $\Delta P^{\mathrm{IAC}}_{T_{set}+1}$, the scheduling strategy does not immediately trigger an adjustment of the temperature setpoint. Instead, it decreases the temperature setpoint by 1 °C only after the power deviation exceeds $\Delta P^{\mathrm{IAC}}_{T_{set}+1.5}$. If the power deviation subsequently drops, it must decrease to $(\Delta P^{\mathrm{IAC}}_{T_{set}+1} + \Delta P^{\mathrm{IAC}}_{T_{set}-1})/2$ before the temperature setpoint can be increased by 1 °C. By introducing upper and lower threshold intervals, this piecewise hysteresis scheduling strategy effectively mitigates the frequent temperature scheduling actions caused by minor fluctuations in the PV output. Consequently, while guaranteeing the aggregate response flexibility of the fleet, it significantly enhances user comfort and regulation stability.

(2) Response Priority Ranking Mechanism

To further enhance the precision and energy efficiency of the fleet's aggregate response, and considering the "activation delay" characteristic inherent in the power regulation of variable-frequency AC compressors, this paper introduces a priority ranking mechanism based on response timeliness into the temperature setpoint regulation strategy. By constructing a response priority index Γ_{IAC}, target units with greater response potential are screened prior to AC temperature adjustments, thereby achieving differentiated regulation.

$$\Gamma_{IAC} = w_1 \cdot \left(\frac{|\Delta T_q|}{T_\delta} \right) + w_2 \cdot (1 - \frac{AT_q}{AT_{\max}}) \tag{32}$$

where ΔT_q represents the difference between the current indoor temperature and the temperature setpoint of the AC; AT_q and $AT_{\max}$ are the estimated and maximum activation time delays corresponding to this temperature difference, respectively; and w_1, w_2 are weighting coefficients used to balance the emphasis on response speed versus user comfort.

Based on the priority values, the candidate ACs are ranked. Considering user comfort and willingness, the top L units are selected to enter the regulation task queue, where L can be estimated according to the current power regulation target. Subsequently, the temperature setpoints are adjusted sequentially based on the priority order, ensuring that the regulation process is graduated and controllable. By integrating the piecewise hysteresis logic with the response priority ranking mechanism, this scheduling framework fully exploits the potential of variable-frequency AC fleets in mitigating PV power fluctuations. It effectively enhances the response speed and precision of the regulation strategy while simultaneously avoiding ineffective regulation and comfort disturbances during fleet scheduling. Consequently, this provides robust support for achieving the grid-friendly integration and local accommodation of distributed PV systems.

3.4. Coordinated Scheduling Strategy for Large-Scale Heterogeneous Air Conditioning Clusters

Against the backdrop of frequent PV output fluctuations and limited energy storage capacity within the park, fully exploiting the response capabilities of multi-type AC loads is of immense significance for constructing a flexible and adjustable demand-side resource system. Based on the in-depth analysis of the modeling characteristics and response mechanisms of fixed-frequency and variable-frequency AC fleets in the preceding sections, this paper proposes a coordinated scheduling strategy for large-scale fixed- and variable-frequency ACs aimed at mitigating PV fluctuations. This strategy aims to enhance the overall regulation precision, reduce regulation latency, and guarantee user comfort through a differentiated response regulation mechanism.

(1) General Scheduling Framework

This strategy is based on the unified framework of "response priority ranking + temperature setpoint adjustment." Because fixed-frequency ACs feature rapid response speeds and large power adjustment magnitudes but coarser regulation granularity, whereas variable-frequency ACs possess the advantages of being continuously adjustable with fine-

grained responses but suffer from activation delays, a hierarchical regulation approach of "fixed-frequency first, variable-frequency second" is adopted for the coordinated response. The fixed-frequency AC fleet, with its strong response capability, is prioritized for dispatch to execute the primary regulation tasks. When its regulation capacity is insufficient to satisfy the current power deviation, the variable-frequency AC fleet is subsequently dispatched to perform compensatory regulation. This mechanism fully accounts for the inherent differences between the two—namely, the rapid response but limited precision of fixed-frequency ACs, and the fine-grained response but delayed activation of variable-frequency ACs—thereby achieving functional complementarity and regulatory coupling between the two types of ACs.

(2) Priority Regulation Strategy for Fixed-Frequency AC Fleets

Due to their characteristics of clear ON/OFF states and large power step changes, fixed-frequency ACs are highly suitable as the primary response resource for system regulation. Based on the aforementioned response state identification and priority ranking mechanism, the regulation strategy identifies units with high "response value" among the candidate response units—specifically, individual ACs with small current temperature differences and long continuous operating or standby durations. By adjusting their temperature setpoints, the strategy indirectly induces the transition of their compressor ON/OFF states, thereby achieving a rapid reduction or increase in the electrical load.

During each regulation cycle, based on the magnitude of the power deviation $\Delta P_l(t)$, the system prioritizes selecting the top 40% of units with the highest response potential within the fixed-frequency AC fleet to execute a ± 1 °C temperature setpoint adjustment operation. If the resulting response capacity $\Delta P_{ACG}(t)$ satisfies the regulation demand, the scheduling action for the current cycle concludes. Otherwise, the remaining power deviation is allocated to the variable-frequency AC fleet for a compensatory response.

(3) Compensatory Regulation Mechanism for Variable-Frequency AC Fleets

Compared to fixed-frequency ACs, variable-frequency ACs possess advantages such as continuous adjustability, fine granularity in temperature setpoint adjustments, and a lower impact on user comfort. Consequently, they are highly suitable as "fine-grained compensation" units in response regulation. However, due to their activation delay and non-linear regulation characteristics, directly utilizing them as primary response resources could result in regulation lag. Therefore, within this strategy, variable-frequency ACs are primarily employed for the dynamic compensation of the response deficit left by the fixed-frequency ACs.

The regulation process is based on the "piecewise hysteresis temperature difference scheduling strategy." By integrating the activation delay characteristics, it constructs the response priority index Γ_{IAC} and ranks the AC fleet. The top-ranked variable-frequency AC units are screened out, and their temperature setpoints are adjusted on-demand to achieve fine-grained regulation, ensuring that the aggregate response power matches the system's regulation requirements.

(4) Mathematical Formulation of the Coordinated Scheduling Strategy

For any given time step t, the target power deviation $\Delta P_l(t)$ is jointly compensated by the fixed-frequency AC fleet and the variable-frequency AC fleet, which can be expressed as:

$$\Delta P_l(t) = \Delta P_{ACG}(t) - \Delta P_{IACG}(t) \tag{33}$$

where $\Delta P_{ACG}(t)$ represents the regulation power of the fixed-frequency AC fleet; and $\Delta P_{IACG}(t)$ represents the regulation power of the variable-frequency AC fleet. In practical execution, $\Delta P_{ACG}(t)$ is calculated with priority. If $\Delta P_l(t) \leq \Delta P_{ACG}(t)$ is satisfied, the scheduling action is exclusively executed by the fixed-frequency AC fleet. If a residual deviation remains, the remaining portion $\Delta P_{\text{rest}}(t) = \Delta P_l(t) - \Delta P_{ACG}(t)$ is assigned to

the variable-frequency AC fleet to complete the response, thereby forming a dynamic scheduling structure characterized by "layer-by-layer progression and progressive reduction." Through this mechanism, the tracking capability of the park's load response system against PV output disturbances can be significantly enhanced. This reduces the reliance on the energy storage system and achieves maximum source-load coordination and regulation capacity.

3.5. Energy-Power Complementarity Scheduling Strategy for Energy Storage Batteries and Heterogeneous AC Fleets

Once the AC temperature setpoint adjustments are completed, power deviations may temporarily arise within the system due to the inherent time lags in the response processes of the fixed-frequency and variable-frequency AC fleets. To effectively compensate for these transient deviations, real-time charging and discharging of the batteries must be employed for regulation. Consequently, the charging and discharging power of the BESS during this phase can be expressed as:

$$P_{\text{bat}}(t) = \Delta P_l(t) - \Delta P_{ACG}(t) - \Delta P_{IACG}(t) \tag{34}$$

By modulating the output power of the batteries, the frequent fluctuations in PV output can be effectively suppressed, and power compensation can be provided for the time delays and deviations inherent in the response of the AC load clusters. Simultaneously, the AC loads themselves possess a certain degree of regulatory capability; their response capacity can, to a certain extent, reduce the charging/discharging power and energy requirements of the battery system. This achieves a synergistic complementarity between the BESS and the AC loads, enhancing the regulation efficiency and stability of the overall system.

The scheduling flow of the energy-power complementarity between the storage batteries and the AC fleets is illustrated in Figure 8. In the figure, the solid blue line represents the real-time battery power $P_{\text{bat}}(t)$, the dashed black line represents the intertie target power $P_{line}^{m}(t)$, and the solid red line represents the real-time power of the fixed-frequency and variable-frequency AC clusters.

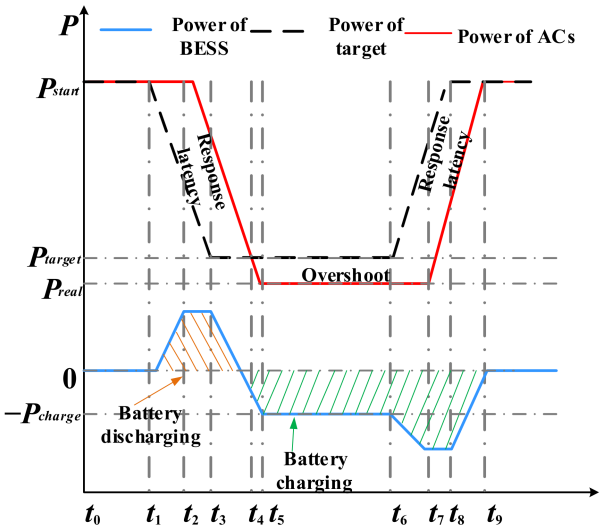

Figure 8. Battery-air conditioning group power energy complementary scheduling.

At time t_1, due to an abrupt drop in PV output, the system must rapidly reduce the total power from the initial value P_{start} to the target value P_{target}. This response process can be divided into two parts: the power compensation from the BESS and the energy regulation from the AC clusters.

(1) Energy Storage Battery Power Compensation

During the periods $t_1 - t_4$ and $t_6 - t_9$, due to the response time lag of the AC clusters, the system is unable to track the variations in intertie power caused by PV output fluctuations in a timely manner. This results in the actual system power deviating from the target value. To bridge the response gap during these phases, the charging and discharging power of the energy storage batteries must be flexibly regulated to provide dynamic compensation for the power deviations caused by the AC response delays:

$$P_{\text{bat}}(t) = P_{\text{line}}^{\text{m}}(t) - P_{\text{ACG}}(t) - P_{\text{IACG}}(t) \tag{35}$$

During the period $t_4 - t_6$, following the temperature setpoint adjustments, the power output of the AC clusters gradually approaches a steady state. However, due to the discrete regulation characteristics of the temperature setpoints, the AC clusters are unable to achieve precise matching with the target power during the load reduction process. This results in a persistent response deviation within the system, which must be addressed by the BESS through the provision of corresponding power compensation. This compensation power is defined as:

$$P_{\text{bat}}(t) = P_{\text{target}} - P_{\text{ACG}}(t) - P_{\text{IACG}}(t) \tag{36}$$

(2) AC Cluster Energy Regulation

Throughout the entire regulation process from $t_1 - t_9$, the AC clusters effectively alleviate the energy release burden that the storage batteries must bear when responding to PV output fluctuations by reducing their own power consumption. This coordinated response mechanism helps mitigate intertie power fluctuations caused by rapid changes in PV output. By providing energy support to the batteries through AC power reduction, the overall stability and operational efficiency of the system are enhanced. The amount of energy regulation provided by the AC clusters can be quantified as:

$$E_{\text{AGG}}(t) = \int_{t_1}^{t_9} (P_{\text{start}} + P_{\text{ACG}}(t) + P_{\text{IACG}}(t) - P_{\text{line}}^{\text{m}}(t))\mathrm{d}t \tag{37}$$

The coordinated scheduling of the BESS and AC clusters establishes a complementarity mechanism between power and energy, fully leveraging the respective advantages of these two types of resources in terms of dynamic response and energy regulation. Compared to scheduling methods that rely solely on AC clusters or energy storage batteries, this integrated scheduling strategy not only tracks the dynamic variations in PV output more rapidly and accurately but also effectively reduces the charging and discharging energy requirements of the battery system. Consequently, it enhances the overall operational efficiency of the system and improves the longevity of its components.

4. Case Study

4.1. Basic Data

The PV output data is sourced from distributed PV power generation facilities located in an industrial park in Jiangsu Province, China, with an installed capacity of 650 kW. To demonstrate the effectiveness of the coordinated scheduling strategy for the BESS and the fixed- and variable-frequency AC fleets in mitigating PV power fluctuations, data from a day exhibiting significant PV volatility is selected as the input. The actual PV output, the smoothed PV output following filtering, and the predicted PV output are illustrated in Figure 9. The sampling interval is set to 1 min, utilizing a total of 6 h of data spanning from 9:00 to 15:00. Furthermore, the ambient temperature of a typical summer day in Jiangsu is adopted as the external environmental temperature, which is also depicted in Figure 7.

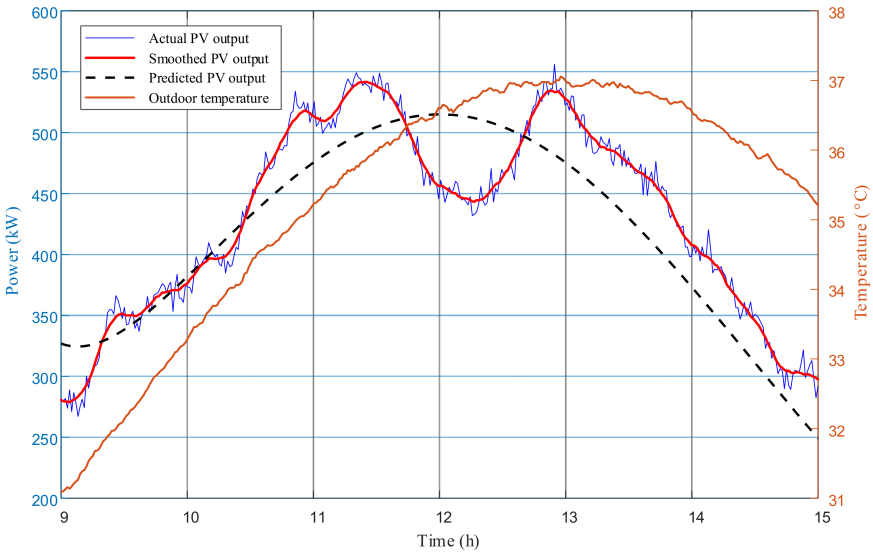

Figure 9. PV actual output, PV predicted output, smooth PV output and outdoor temperature curve.

To verify the effectiveness of the joint scheduling strategy involving heterogeneous AC fleets and energy storage, four case studies are established in this paper. Among them, Case 4 represents the heterogeneous coordinated dispatch method proposed in this study. To facilitate a quantitative comparison with specialized literature under identical boundary conditions, Case 2 and Case 3 are explicitly designed as baseline scenarios representing mainstream existing methods: the former corresponds to approaches focusing on homogeneous AC clusters with discrete ON/OFF control, while the latter represents those with continuous power regulation. The capacity and the initial SOC of the energy storage battery are set to 300 kWh and 40%, respectively. The specific quantities of the fixed-frequency and variable-frequency AC units are detailed in Table 2.

Table 2. Scale of constant frequency air conditioning cluster.

Case	Number of Fixed-Frequency ACs	Number of Variable-Frequency ACs
1	0	0
2	240	0
3	0	240
4	60	180

Case 1: Involves no AC scheduling, relying solely on the charging and discharging of the energy storage battery to mitigate PV power fluctuations.

Case 2: Employs the coordinated scheduling of the energy storage battery and the fixed-frequency AC fleet to mitigate PV fluctuations.

Case 3: Utilizes the coordinated scheduling of the energy storage battery and the variable-frequency AC fleet.

Case 4: Implements the proposed coordinated scheduling of the energy storage battery and the heterogeneous (both fixed- and variable-frequency) AC fleets.

4.2. Simulation Results

The results of the four cases are illustrated in Figure 8, where the visual elements are defined as follows: Blue curve represents the target power, which is the difference between the actual and predicted PV output. Red curve reflects the actual operating power of the intertie after mitigating the PV output using the respective response strategies. Green bars

indicate the charging and discharging power of the BESS (positive values denote charging, negative values denote discharging). Orange and Cyan bars represent the power response behaviors of the fixed-frequency and variable-frequency AC fleets, respectively. Positive values indicate a load increase (achieved by lowering the temperature setpoint), while negative values indicate a load reduction (achieved by raising the temperature setpoint).

In terms of the mitigation effect, the proposed coordinated strategy in Case 4 increases the PV output mitigation rate from 77.16% to 100%, achieving the full absorption of PV fluctuations. Simultaneously, the power standard deviation of the BESS decreases from 48.56 kW to 6.22 kW, the SOC fluctuation range is reduced to 1%, and the total energy throughput drops to 4.02 kWh, representing a reduction of over 90% compared to the baseline scenario. Furthermore, although the number of charge/discharge cycles increases slightly (to 360 cycles), the depth of discharge per cycle is significantly reduced. This results in a milder system operation, which is highly conducive to extending battery life and maintaining thermal management stability. These results indicate that the introduction of heterogeneous AC fleets can substantially diminish the operational intensity of the BESS, enhance the system's regulation precision, and improve the local accommodation capacity. Consequently, this thoroughly verifies the feasibility and superiority of the AC-BESS coordinated mechanism.

Figure 10 shows the simulation results for Case 1, where the system relies exclusively on the BESS to mitigate PV output fluctuations. To track the target power and suppress tie-line power deviations, the BESS frequently operates at its charging and discharging power boundaries across multiple time intervals. Such high-frequency, high-amplitude operation significantly increases the number of charge/discharge cycles, posing a potential threat to battery lifetime and performance stability. Moreover, prolonged operation under extreme conditions may lead to increased thermal management stress and reduced efficiency, thereby compromising the system's long-term sustainability in flexible regulation. Constrained by the rated power limits, the BESS exhibits insufficient regulation capability when confronted with large-magnitude PV fluctuations. When the deviation between actual and forecasted PV output exceeds the maximum charging/discharging capacity, full power compensation cannot be achieved, making it difficult to adequately smooth the PV output. Throughout the entire simulation period, the BESS undergoes persistent high-frequency charge/discharge switching, with its power output consistently operating near the boundary values, resulting in a total energy throughput of 53.50 kWh and a target power tracking error rate of 22.55%. These results indicate that substantial room remains for improving the regulation performance.

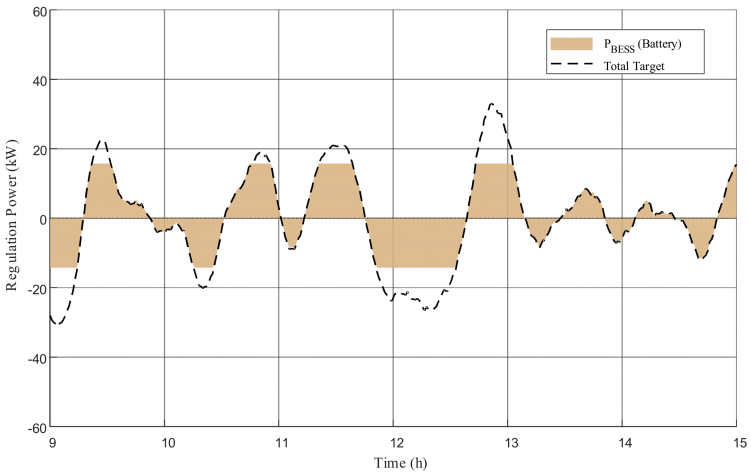

Figure 10. PV power smoothing results with only BESS response.

Figure 11 presents the simulation results for Case 2, which extends Case 1 by incorporating a fixed-frequency AC cluster for coordinated dispatch. The fixed-frequency AC cluster performs temperature setpoint adjustments based on a response-state prioritization mechanism—individual AC units are classified into hierarchical response sets according to their current operating status, temperature deviation, and ON/OFF lockout state and are then ranked by priority. The temperature setpoints of selected units are adjusted accordingly to achieve precise regulation of the aggregate cluster power. Results demonstrate that the introduction of the fixed-frequency AC cluster reduces the BESS energy throughput from 53.50 kWh to 48.66 kWh. Owing to their absence of activation delay and rapid ON/OFF switching capability, fixed-frequency ACs can instantaneously realize step-wise load increases or decreases upon receiving dispatch commands, thereby effectively alleviating the regulation burden on the BESS.

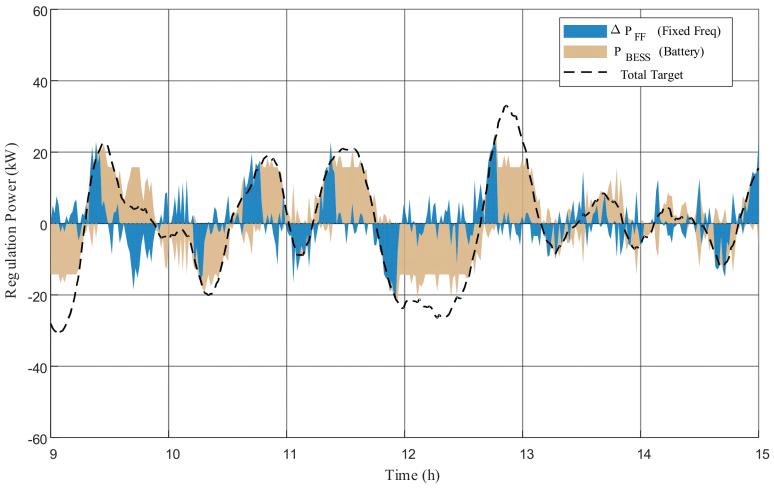

Figure 11. PV power smoothing results with the response of BESS and fixed-frequency AC clusters.

However, the response sustainability of fixed-frequency ACs is constrained by their inherent operational mechanisms. During continuous regulation, certain AC units gradually enter the minimum ON/OFF time lockout period and become temporarily unable to switch states again, leading to a progressive shrinkage of the dispatchable resource pool. Furthermore, the response magnitude of fixed-frequency ACs is structurally limited—regardless of whether the temperature setpoint is adjusted by ±1 °C or ±2 °C, the actual load response of an individual unit does not vary substantially, resulting in insufficient marginal response capacity for subsequent regulation actions. Consequently, under prolonged and large-amplitude fluctuation conditions, the standalone regulation capability of the fixed-frequency AC cluster remains subject to certain limitations.

Figure 12 presents the simulation results for Case 3. Case 3 employs a coordinated dispatch scheme integrating the BESS with a variable-frequency (VF) AC cluster. The VF AC cluster performs power regulation based on a temperature-difference-driven piecewise hysteresis scheduling strategy. By introducing upper and lower threshold intervals, this strategy effectively avoids frequent temperature adjustments triggered by minor PV fluctuations, thereby significantly enhancing user comfort and regulation stability while preserving the aggregate response flexibility of the cluster. The FF AC cluster remains in autonomous operation throughout this case and does not participate in dispatch control.

Simulation results show that the introduction of the VF AC cluster further reduces the BESS energy throughput to 43.73 kWh, with a target power tracking error rate of 12.81%. Throughout the regulation process, the VF AC cluster maintains a relatively stable and continuous regulation capability, providing substantial flexible regulation headroom for the system. Owing to the piecewise hysteresis mechanism, the AC cluster remains idle

when the target power deviation is small and initiates regulation only after the fluctuation amplitude exceeds the preset threshold, thereby effectively avoiding unnecessary frequent actions. However, due to user comfort considerations and the inherent activation delay characteristic of VF AC compressors, the response speed during the initial regulation phase is relatively slow. When PV fluctuations are severe and regulation demands are urgent, the response timeliness of the VF AC cluster faces certain challenges.

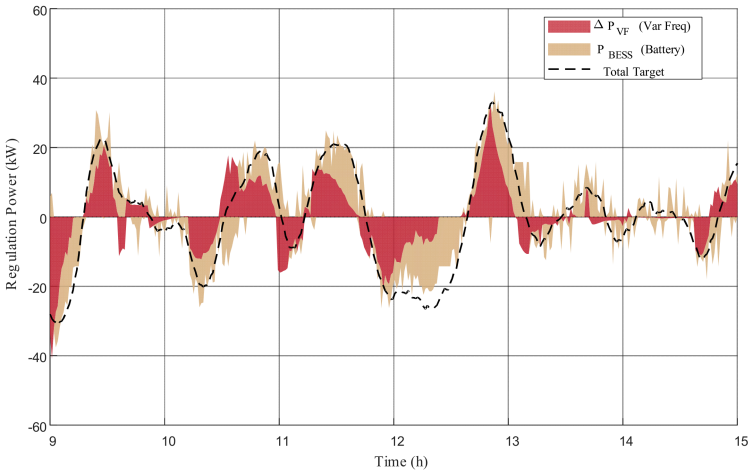

Figure 12. PV power smoothing results with the response of BESS and variable-frequency AC clusters.

Figure 13 illustrates the system's rapid mode transition from "load-increasing for PV accommodation" to "load-shedding for fluctuation tracking" during 12:00–13:00, when PV output drops sharply. In the preceding period (10:00–12:00), the fixed-frequency (FF) AC cluster served as the primary accommodation resource. Because FF ACs in the free layer have no activation delay and possess rapid ON/OFF capabilities, they are prioritized to achieve instantaneous load regulation through minor adjustments to their temperature setpoints, effectively absorbing surplus PV power. However, as the response continues, some FF AC units temporarily lose their response capability due to entering the lockout intervals formed by minimum ON/OFF time constraints.

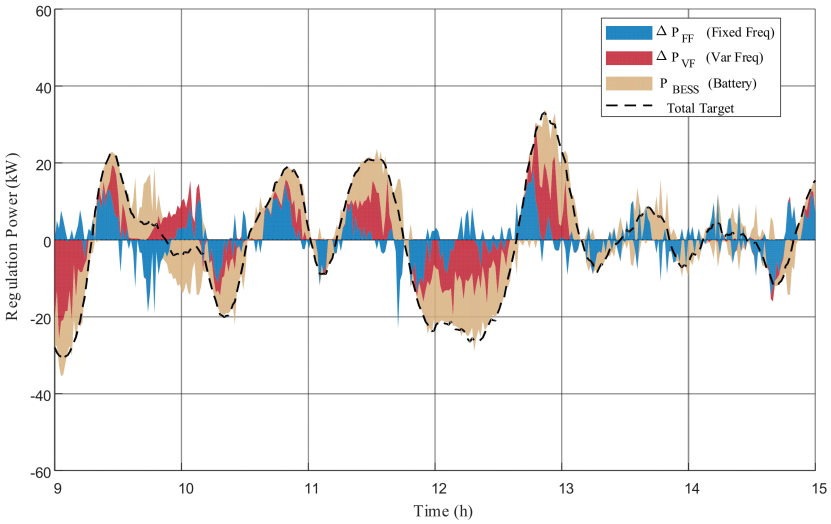

Figure 13. PV power smoothing results with the response of BESS and mixed fixed- and variable-frequency AC clusters.

At this point, as PV output declines steeply after 12:00, the variable-frequency (VF) AC cluster takes over to provide compensatory regulation. Although VF ACs involve a

certain activation time delay—which limits their regulation efficiency in the initial stage—they possess the inherent advantages of continuous adjustability and smooth response. Configured as the secondary regulation layer, they intervene in a timely manner when the adjustable potential of the FF ACs is insufficient. Their temperature setpoints are rapidly raised, yielding an aggregate power reduction of 165.91 kW. This intervention seamlessly forms a dual-layer response mechanism characterized by a "fast–slow combination and rigid–flexible complementarity," achieving smooth and deep load curtailment.

This coordinated strategy effectively enhances the flexibility and continuity of the system's overall regulation, providing a crucial guarantee for the efficient absorption of PV output disturbances. During this transition period, the BESS provides only auxiliary discharging compensation at an average power of 4.13 kW. Although time delays and localized power overshoot phenomena during the response process cannot be completely avoided due to the physical constraints of the AC units, the overall regulation performance continues to exhibit a high degree of stability. Consequently, the charging/discharging magnitude of the BESS is significantly reduced compared with Cases 1–3. Statistical results show that the BESS energy throughput in Case 4 is merely 42.74 kWh, representing reductions of 20.1% relative to Case 1 and 12.2% relative to Case 2, while the target power tracking error rate drops to 5.19%. These results comprehensively validate the effectiveness of the proposed strategy: high-precision power tracking is achieved while substantially reducing the operational intensity of the BESS.

By hierarchically dispatching the heterogeneous AC clusters, the proposed strategy effectively decouples the power and energy compensation requirements. The fixed-frequency units, acting as the primary discrete responders, absorb the high-amplitude power shocks. Concurrently, the variable-frequency units provide continuous mid-frequency buffering. This synergistic decoupling ensures that the BESS is solely reserved for mitigating high-frequency, low-energy residual tracking errors caused by the inherent physical constraints of the AC equipment. Furthermore, the thermodynamic inertia of the buildings is fully mobilized as a virtual low-pass filter, transforming abrupt PV fluctuations into smooth indoor temperature variations within the acceptable deadband. This physical transformation is the fundamental reason why the BESS energy throughput is drastically reduced, thereby offering a highly sustainable and economically viable approach to localized PV accommodation.

Based on this comprehensive analysis, the proposed flexible resource coordinated regulation system of "battery-heterogeneous AC fleet composite energy storage," oriented towards mitigating PV output fluctuations, achieves remarkable results in smoothing fluctuations and alleviating the operational pressure on the BESS. It effectively diminishes the dynamic stress on the BESS, thereby reducing the overall system costs of the PV-storage park. This demonstrates excellent application prospects and engineering promotion value, providing a realistic and feasible new pathway for distributed source-load coordinated scheduling under the high-penetration integration of renewable energy.

5. Conclusions

To address the issues of significant differences in response characteristics and the lack of coordinated regulation mechanisms when heterogeneous AC fleets participate in mitigating PV fluctuations, this paper considers the distinct response processes of two types of ACs: the "discrete ON/OFF and minimum runtime constraints" of fixed-frequency ACs, and the "activation delay and non-linear regulation" of variable-frequency ACs. Accordingly, a dynamic regulation model for fixed-frequency ACs based on ON/OFF state evolution and response priority ranking, alongside a response model for variable-frequency ACs based on piecewise hysteresis and activation time modeling, were established. These models accurately depict the dynamic behavioral boundaries and physical constraints of

both AC types during actual operation. By integrating the BESS within the PV park, this paper proposes an operational regulation strategy for a "battery-heterogeneous AC fleet composite energy storage" system aimed at PV accommodation. The main conclusions are as follows:

(1) The proposed hierarchical regulation structure—characterized by "fixed-frequency AC priority, variable-frequency AC compensation, and BESS backup"—establishes a coordinated regulation mechanism for the composite energy storage system in PV parks. This mechanism significantly enhances the system's tracking precision and regulation flexibility against PV disturbances, effectively suppressing the power deviations caused by the discontinuous regulation and response time delays of the AC fleets.

(2) Comparative simulations conducted under typical PV output scenarios demonstrate that the proposed coordinated strategy reduces the target power tracking error rate to 5.19%. Furthermore, the power standard deviation of the BESS decreases from 10.48 kW to 8.59 kW, the SOC fluctuation range narrows from 3.86% to 2.81%, and the total charge/discharge energy throughput drops from 53.50 kWh to 42.74 kWh, representing a reduction of 20.1% compared to the baseline strategy. These quantitative results rigorously verify the strategy's effectiveness in alleviating the operational pressure on the BESS while maintaining high-precision power tracking, as well as enhancing the local PV accommodation capacity and the overall operational sustainability of the park.

While this study effectively validates the proposed framework under severe summer PV fluctuation scenarios, future research will conduct extended simulations to explore the model's capabilities under diverse seasonal climates and larger-scale multi-park grid topologies.

Author Contributions: Methodology, X.D. and H.Y.; Software, S.W. and X.L.; Formal analysis, X.L., Q.F., X.D. and H.Y.; Resources, S.W. and C.J.; Data curation, X.L. and C.J.; Writing—original draft, S.W. and X.L.; Writing—review and editing, Y.Z., Q.F., X.D. and H.Y.; Supervision, S.W., X.L., Y.Z., C.J., X.D. and H.Y.; Project administration, Y.Z.; Funding acquisition, Y.Z. All authors have read and agreed to the published version of the manuscript.

Funding: This work is supported by the National Natural Science Foundation of China (52407107) and the Natural Science Foundation of the Jiangsu Higher Education Institutions of China (23KJB470014).

Data Availability Statement: The data presented in this study are available on request from the corresponding author due to legal and privacy reasons.

Conflicts of Interest: Author Y.Z. was employed by Inner Mongolia Electric Power (Group) Co., Ltd. and author Q.F. was employed by the State Grid Zhejiang Electric Power Co., Ltd. The remaining authors declare that the research was conducted in the absence of any commercial or financial relationships that could be construed as a potential conflict of interest.

Nomenclature

The following symbols and abbreviations are used in this manuscript:

R_a	Indoor air thermal resistance	°C/kW
C_a	Indoor air thermal capacitance	$(\text{kW}\cdot\text{h})\cdot{}^\circ\text{C}^{-1}$
R_m	Indoor solid thermal resistance	°C/kW
C_m	Indoor solid thermal capacitance	$(\text{kW}\cdot\text{h})\cdot{}^\circ\text{C}^{-1}$
$T_a(t)$	Indoor air temperature	°C
$T_m(t)$	Indoor solid temperature	°C
$T_o(t)$	Outdoor temperature	°C
$Q(t)$	Heating power of air conditioner	kW
r	Characteristic root	

b, c	Coefficients of the characteristic equation	
$S(t_k)^{(h)}$	Air conditioner operating state	0, 1
$T_{set}^{(h)}$	Air conditioner temperature setpoint	°C
$T_{\delta}^{(h)}$	Temperature deadband	°C
$S_{on}^{(h)}$	Cooling state	0, 1
$S_{off}^{(h)}$	Standby state	0, 1
$P^{(h)}$	Air conditioner power consumption	kW
$P_{on}^{(h)}$	Cooling power	kW
$P_{off}^{(h)}$	Standby power	kW
$SOC(t)$	Initial state of charge at time t	
$E_{BESS}(t)$	Charging energy of the battery at time t	kWh
R_{BESS}	Rated capacity of the battery energy storage system	kWh
$SOC_{\min}$	Minimum state of charge	
$SOC_{\max}$	Maximum state of charge	
$P_{charge,\max}$	Maximum charging power of the battery	kW
$P_{discharge,\max}$	Maximum discharging power of the battery	kW
R_{inv}	Rated capacity of the inverter	kWh
P_{charge}	Charging power of the battery	kW
$P_{discharge}$	Discharging power of the battery	kW
$E_{BESScha,\max}(t)$	Maximum charging energy of the BESS	kWh
$E_{BESSdis,\max}(t)$	Maximum discharging energy of the BESS	kWh
$P_{PV}^{s}(t)$	Smoothed PV power output	kW
n	Number of sampling points in the moving average	
$\Delta P_l(t)$	Power deviation of the tie-line	kW
$P_{line}(t)$	Actual tie-line power	kW
$P_{line}^{m}(t)$	Forecast tie-line power	kW
$P_{bat}(t)$	Real-time battery power	kW
$P_{ACG}(t)$	Real-time total power of fixed-frequency AC cluster	kW
$P_{IACG}(t)$	Real-time total power of IAC cluster	kW
$P_L(t)$	Real-time aggregate power of other loads	kW
$P_{PV}^{m}(t)$	Forecast PV power output	kW
$P_{ACG}^{m}(t)$	Forecast total power of fixed-frequency AC cluster	kW
$P_{IACG}^{m}(t)$	Forecast total power of IAC cluster	kW
$P_L^{m}(t)$	Forecast aggregate power of other loads	kW
P_{target}	Target power	kW
$\Gamma_q^{\downarrow}$	Load shedding priority	
$w_1^{\downarrow}$, $w_2^{\downarrow}$	Weighting coefficient	
ΔT_q	Temperature deviation	°C
τ_q^{on}	Elapsed operating time	s
$\tau_{\max}^{on}$	Maximum operating time	s
$\Gamma_q^{\uparrow}$	Load increase priority	
$w_1^{\uparrow}$, $w_2^{\uparrow}$	Weighting coefficient	
τ_q^{off}	Elapsed standby time	s
$\tau_{\max}^{off}$	Maximum off time	s
$s_i(t)$	Operating state of AC i at time t	0, 1
$P_{AC,i}$	Rated power of fixed-frequency AC	kW
$\Delta P_{T_{set}+\Delta T_{set}}^{IAC}$	Power variation after adjusting IAC set temperature	kW
M_{IAC}	Operating mode of IAC	0, 1
η_{IAC}	Energy efficiency ratio of IAC	
Γ_{IAC}	Response priority index	
AT_q	Estimated time activation value corresponding to temperature difference	s

$AT_{\max}$	Maximum time activation value corresponding to temperature difference	s
w_1, w_2	Weighting coefficient	
$\Delta P_l(t)$	Target power deviation	kW
$\Delta P_{ACG}(t)$	Regulation power of fixed-frequency AC group	kW
$\Delta P_{IACG}(t)$	Regulation power of IAC group	kW

Abbreviations

The following abbreviations are used in this manuscript:

PV	Photovoltaic
AC	Air conditioning
BESS	battery energy storage systems
ETP	Equivalent Thermal Parameter
RC	Resistor–Capacitor
SOC	State of Charge

References

1. Huang, R.; Wang, P.; Zhang, S.; Ren, Z.; Pu, L. Power system transition pathways in mega-cities under the 'Dual Carbon' targets: A multi-temporal case study of Beijing in China. *Renew. Energy* **2026**, *260*, 125221. [CrossRef]
2. Gupta, P.D.; Habeeb, N.; Shah, R.; Amjady, N. Aggregation of Distributed Energy Resources and Energy Storage Systems in Active Distribution Networks: A Critical Review. *Energies* **2026**, *19*, 1579. [CrossRef]
3. Nitta, N.; Wu, F.; Lee, J.T.; Yushin, G. Li-ion battery materials: Present and future. *Mater. Today* **2015**, *18*, 252–264. [CrossRef]
4. Vetter, J.; Novák, P.; Wagner, M.R.; Veit, C.; Möller, K.-C.; Besenhard, J.O.; Winter, M.; Wohlfahrt-Mehrens, M.; Vogler, C.; Hammouche, A. Ageing mechanisms in lithium-ion batteries. *J. Power Sources* **2005**, *147*, 269–281. [CrossRef]
5. Feng, X.; Ouyang, M.; Liu, X.; Lu, L.; Xia, Y.; He, X. Thermal runaway mechanism of lithium ion battery for electric vehicles: A review. *Energy Storage Mater.* **2018**, *10*, 246–267. [CrossRef]
6. Lu, N. An Evaluation of the HVAC Load Potential for Providing Load Balancing Service. *IEEE Trans. Smart Grid* **2012**, *3*, 1263–1270. [CrossRef]
7. Che, Y.; Yang, J.; Zhao, Y.; Xue, S. Control Strategy for Inverter Air Conditioners under Demand Response. *Processes* **2019**, *7*, 407. [CrossRef]
8. Che, Y.; Yang, J.; Zhou, Y.; Zhao, Y.; He, W.; Wu, J. Demand Response from the Control of Aggregated Inverter Air Conditioners. *IEEE Access* **2019**, *7*, 88163–88173. [CrossRef]
9. Hao, H.; Sanandaji, B.M.; Poolla, K.; Vincent, T.L. Aggregate Flexibility of Thermostatically Controlled Loads. *IEEE Trans. Power Syst.* **2015**, *30*, 189–198. [CrossRef]
10. Dong, L.; Wu, Q.; Hong, J.; Wang, Z.; Fan, S.; He, G. An adaptive decentralized regulation strategy for the cluster with massive inverter air conditionings. *Appl. Energy* **2023**, *330*, 120304. [CrossRef]
11. Bianchini, G.; Casini, M.; Pepe, D.; Vicino, A.; Zanvettor, G.G. An integrated model predictive control approach for optimal HVAC and energy storage operation in large-scale buildings. *Appl. Energy* **2019**, *240*, 327–340. [CrossRef]
12. Hu, Z.; Gao, Y.; Sun, L.; Mae, M.; Imaizumi, T. Improved robust model predictive control for residential building air conditioning and photovoltaic power generation with battery energy storage system under weather forecast uncertainty. *Appl. Energy* **2024**, *371*, 123652. [CrossRef]
13. Matiašovský, P. The equivalent thermal parameters, their analytical and experimental identification. *Sol. Energy Mater. Sol. Cells* **1992**, *27*, 119–126. [CrossRef]
14. Pan, D.; Dong, L.; Fan, S.; Huang, Y.; Yang, S.; He, G. Identification Method for Air-conditioning-Building Electrothermal Coupling System Based on Second-order Equivalent Thermal Parameter Analytical Solution. *Autom. Electr. Power Syst.* **2023**, *47*, 77–87. [CrossRef]